KTH Electrical Engineering

Characterization and Linearization of Multi-channel RF Power Amplifiers

SHOAIB AMIN

Licentiate Thesis
Electrical Engineering
School of Electrical engineering
KTH
Stockholm, Sweden, 2015

TRITA-EE 2015:001
ISSN 1653-5146
ISBN 978-91-7595-388-5

KTH - Electrical Engineering
Signal Processing
SE-100 44 Stockholm, SWEDEN

Akademisk avhandling som med tillstånd av Kungl Tekniska högskolan framlägges till offentlig granskning för avläggande av teknologie licentiatexamen fredagen den 23 Jan 2015 klockan 10.00 i hörsal 99132, Kungsbäcksvägen 47, Gävle.

© Shoaib Amin, January 2015

Tryck: Universitetsservice US AB

Abstract

The demands for high data rates and broadband wireless access require the development of wireless systems that can support wide and multi-band signals. To deploy these signals, new radio frequency (RF) front-ends are required which impose new challenges in terms of power consumption efficiency and sources of distortion e.g., nonlinearity. These challenges are more pronounced in power amplifiers (PAs) that degrade the overall performance of the RF transmitter.

Since it is difficult to optimize the linearity and efficiency characteristics of a PA simultaneously, a trade-off is needed. At high input power, a PA exhibits high efficiency at the expense of linearity. On the other hand, at low input power, a PA is linear at the expense of the efficiency. To achieve linearity and efficiency at the same time, digital pre-distortion (DPD) is often used to compensate for the PA nonlinearity at high input power. In case of multi-channel PAs, input and output signals of different channels interact with each other due to cross-talk. Therefore, these PAs exhibit different nonlinear behavior than the single-input single-output (SISO) PAs. The DPD techniques developed for SISO PAs do not result in adequate performance when used for multi-channel PAs. Hence, an accurate behavioral modeling is essential for the development of DPD for multi-channel RF PAs.

In this thesis, we propose three novel behavioral models and DPD schemes for nonlinear multiple-input multiple-output (MIMO) transmitters in presence of cross-talk. A study of the source of cross-talk in MIMO transmitters have been investigated to derive simple and powerful modeling schemes. These models are extensions of a SISO generalized memory polynomial model. A comparative study with a previously published MIMO model is also presented. The effect of coherent and partially non-coherent signal generation on DPD performance is also highlighted. It is shown experimentally that with partially non-coherent signal generation, the performance of the DPD degrades compared to coherent signal generation.

In context of multi-channel RF transmitters, PA behavioral models and DPD schemes suffer from a large number of model parameters with the increase in nonlinear order and memory depth. This growth leads to high complexity model identification and implementation. We have designed a DPD scheme for MIMO PAs using a sparse estimation technique for reducing model complexity. This technique also increases the numerical stability when linear least square estimation model identification is used.

A method to characterize the memory effects in a nonlinear concurrent dual-band PAs is also presented. Compared to the SISO PAs, concurrent dual-band PAs are not only affected by intermodulation distortions but also by cross-modulation distortions. The characterization of memory effects in concurrent dual-band transmitter is performed by injecting a two-tone test signal in each input channel of the transmitter. Asymmetric energy surfaces are introduced for the intermodulation and cross-modulation products, which can be used to identify the power and frequency regions where the memory effects are dominant.

Acknowledgments

Before discussing technical details, I would like to take the opportunity to thank people without whom I would not have achieved this milestone.

First and foremost, I owe great thanks to my supervisors, Prof. Daniel Rönnow and Prof. Peter Händel, for giving me the opportunity to pursue the PhD and trusting in me. Their encouragement has been invaluable. Special thanks to Prof. Wendy Van Moer and Dr. Per N. Landin for the time they invested in discussing and working with me.

I also wish to thank Dr. Charles Nader, Dr. Javier Ferrer Coll and Dr. Sathyaveer Prasad for the light discussions during their time over in University of Gävle. Thanks to all the PhD. fellows in the electronic department in Gävle for sharing all ups and downs: Mohammed Hamid, Efrain Zenteno, Usman Haider, Indra, Zain Ahmed Khan and Mahmoud Alizadeh.

My parents Mian Mohammad Amin and Khalida Amin, I know that it was not easy for you to tolerate my absence from past 11 years, your love, support and prayers through out my life was the only source of encouragement. My siblings, Faisal, Aysha, Shumyila and Shumyil, thanks for sharing all the happiness and supporting my quest for PhD. Finally my lovely wife Yumna and my adorable daughter Mishaal, I can not describe in words the love you have brought in my life.

Shoaib Amin
Gävle, January, 2015.

Contents

Part I

Introduction

Chapter 1

Introduction

Advancement in the modulation techniques and radio access technologies are giving raise to high speed mobile access for users. However, this trend is increasing the complexity of RF transmitters. The continued quest for dynamic and flexible radio networks challenges the RF designers to develop novel radio transmitters which are capable of processing multi-channel and frequency aggregated multi-carrier communication signals.

These new requirements make RF front-end implementation more complex and challenging when combined with the requirement of 'green technology' which requires high power efficiency. Different hardware cascaded together and optimized for each standard can be employed to support multi-band standards. However, this solution will dramatically increase the deployment cost of the wireless network and decrease its flexibility which contradicts with modern wireless evolution [1]. A more realistic solution for future wireless systems is to use a multi-channel RF transmitter e.g. a MIMO and concurrent multi-band transmitter to support multi-band, multi-carrier signals simultaneously.

The PAs in the RF front-end are mainly responsible for the high power consumption. Therefore, if the PAs are not operating efficiently, a large part of the provided power is dissipated as heat. During the past years, advanced PA design techniques in hardware such as Doherty [2–4] and envelope tracking [5,6] have been applied to improve the efficiency of the RF PA. Unfortunately, with the increase in efficiency, the signal distortions produced by the PA also increase which results in a degraded quality of the transmitted signals. Numerous techniques have been developed to model nonlinear distortions in PAs. One well known technique for modeling nonlinearities of a system is behavioral modeling.

Behavioral modeling is a black box approach used for modeling the nonlinear behavior of a system using measured input-output signals. These models are frequently used for system simulations [7,8] and are cost effective solution for predicting system performance compared to the circuit simulations. Moreover, behavioral models are also used for DPD [9–12], which is applied to increase the linearity of the

PA. DPD incorporates a nonlinear function before the PA to preprocess the input signal such that the new cascaded system i.e., DPD+PA becomes approximately a linear memoryless system. It should be noticed that the accurate behavioral modeling of a PA provides an effective prediction of its nonlinear and dynamic behavior. Therefore, behavioral modeling is an important step for the formulation of the DPD algorithm of the PA.

There are numerous behavioral models starting from high complexity models such as Volterra series [13–15] and neural networks [16, 17], to low complexity schemes such as memory polynomials models [18–20] which are reduced forms of the Volterra series. Dynamic behavioral models may give an insight into the memory effects of an RF PA, where it should be pointed out that memory effects are equivalent to frequency dependency of the PA within the signal bandwidth [21]. Thus, a commonly used technique to quantify the memory effects in SISO nonlinear systems is a scanned two-tone test [22–26].

Until the last few years, all behavioral models and DPD schemes of RF PAs dealt with single-band scenarios; these models could not be used for multi-channel transmitters without severe performance degradation. Therefore, re-designing an RF front-end for supporting multi-channel operations imposes new efficiency and linearity challenges. Starting from mature SISO modeling and DPD techniques, researchers are motivated to extend this knowledge to MIMO and concurrent multi-band RF PAs.

In recent years, efforts have been made to develop behavioral models and DPD schemes for MIMO [27, 28] and concurrent dual-band transmitters [29, 30]. In [31], continuous time domain SISO Volterra series [13] is extended to a MIMO Volterra series for modeling time invariant dynamic nonlinear MIMO system with fading memory. However, characterization and linearization of nonlinear multi-channel RF transmitters is in an early stage and, thus, require more research efforts for developing new modeling algorithms and methods for the characterization and mitigation of nonlinear effects in multi-channel PAs.

In this thesis, we have studied and addressed three challenges that one faces in the mitigation and characterization of nonlinear effects in multi-channel RF transmitters. First, we discuss the sources of cross-talk and nonlinear effects in multi-channel RF transmitters which require new behavioral modeling/DPD schemes. Second, the dimensionality issue in multi-channel PA behavioral/DPD models is discussed, which increases with the nonlinearity order and memory taps, leading to a larger number of coefficients and lastly, a method for quantifying the memory effects in multi-channel RF transmitters is discussed.

1.1 Thesis contribution

The work presented in this thesis relates to the characterization and digital modeling of MIMO and concurrent dual band transmitters. This work is based upon

the papers published and submitted to the international journals and conferences. The contribution of this thesis is based on 3 papers.

Paper A: Presents three novel behavioral models and DPD algorithms for a nonlinear 2×2 MIMO PA in the presence of cross-talk. The paper highlights different types of cross-talk effects denoted as linear, nonlinear and linear-nonlinear cross-talk. The effect of partially non-coherent and coherent signal generation on the performance of DPD was also studied. Furthermore, a comparative study with a previously published model for a 2×2 MIMO PA was also performed. The paper is summarized in chapter 4.

The author of this thesis was the main contributor of this paper and performed the experimental work and major part in developing the models. The measurement results were presented according to the insight given by the co-authors. The phase noise analysis for partially non-coherent and coherent signal generation was performed by Per N. Landin, Peter Händel and Daniel Rönnow.

Paper B: Proposes a method for reducing the number of parameters in the DPD model of a 2×2 MIMO PA. In this paper, the complex baseband MIMO Volterra series is used as an inverse model for the linearization of a 2×2 MIMO PA. The paper illustrates that by using a basis pursuit algorithms, the total number of model parameters can be reduced while maintaining the DPD performance. The paper is summarized in chapter 4.

The author of this thesis was involved in part of experimental setup and manuscript writing. The major part of basis pursuit was done by Efrain Zenteno. The other co-authors were involved in refining and pointing out the focus of the paper.

Paper C: Proposes a method for characterizing the memory effects in a nonlinear concurrent dual-band PA. Compared to a SISO nonlinear transmitter, the output signal is not only affected by the intermodulation products but also by cross-modulation products which are generated by the nonlinear interaction of input signals at different carrier frequencies. The method proposed in this paper can be used to study and quantify the memory effects in concurrent dual-band PA as well as MIMO PA. Moreover, the method can also be used to tune the parametric memory polynomial models for nonlinear order and memory depth. The paper is summarized in chapter 5.

The author of this thesis was the main contributor of this paper and performed the experimental work and writing the manuscript. The results were analyzed with the insights given by Daniel Rönnow and Wendy Van More. Moreover, the manuscript was reviewed and refined by the co-authors.

Papers included in the thesis

The papers included in this thesis are listed bellow:

- **Paper A:** Shoaib Amin, Per N. Landin, Peter Händel and Daniel Rönnow, "Behavioral Modeling and Linearization of Crosstalk and Memory Effects in RF MIMO Transmitters," IEEE Transactions on Microwave Theory and Techniques,vol. 62, no.4, pp. 810-823, Apr., 2014.
- **Paper B:** Efrain Zenteno, Shoaib Amin, Magnus Isaksson, Daniel Rönnow and, Peter Händel, "Combating the Dimensionality of Nonlinear MIMO Amplifier Predistortion by Basis Pursuit", 44^{th} European Microwave Conference, pp. 833-836, Oct., 2014.
- **Paper C:** Shoaib Amin, Wendy Van Moer, Peter Händel and Daniel Rönnow,"Characterization of a Concurrent dual-band Power Amplifier using a dual-tone excitation signals," IEEE Transactions on Instrumentation and Measurement, submitted, Oct., 2014.

1.2 Acronyms

ACEPR	:	Adjacent channel error power ratio
ACPR	:	Adjacent channel power ratio
ADC	:	Analog to digital converter
CM	:	Cross modulation
DLA	:	Direct learning architecture
DPD	:	Digital pre-distortion
DUT	:	Device under test
EGMPNLC	:	Extended generalized memory polynomial for nonlinear cross-talk
GMP	:	Generalized memory polynomials
GMPLC	:	Generalized memory polynomial for linear cross-talk
GMPNLC	:	Generalized memory polynomial for nonlinear cross-talk
IF	:	Intermediate frequency
ILA	:	Indirect learning architecture
IM	:	Intermodulation
LASSO	:	Least-absolute shrinkage and selection operator
LO	:	Local oscillator
LSE	:	Least square estimate
MIMO	:	Multiple-input Multiple-output
NMSE	:	Normalized mean square error
PA	:	Power amplifier
PAPR	:	Peak to average power ratio
PH	:	Parallel Hammerstein
RF	:	Radio Frequency
R&S	:	Rohde & Schwartz
SISO	:	Single-input single-output
VSG	:	Vector signal generator
WCDMA	:	Wideband code division multiple access

Chapter 2

Modeling Nonlinearities in Multi-channel RF Systems

To characterize a complete nonlinear system or a section of such a system, behavioral modeling is one possibility. In this type of system modeling, the device under test (DUT) being modeled is considered as a black-box, i.e., in principle the modeling information is completely contained in the external response of the DUT and no knowledge of the internal structured of the DUT is required. Due to this property, the model parameters can be extracted effectively. Behavioral models of DUTs provide an effective way to predict the performance of a system. Moreover, behavioral models are also used to compensate nonlinearities in a system using indirect learning architecture (ILA) [32] and direct learning architecture (DLA) [33].

Over the years, in electrical engineering, Volterra series have been used to describe the nonlinear behavior of a variety of nonlinear dynamic time-invariant systems with fading memory [34, 35]. In wireless systems, particularly in base-stations, research emphasis was mainly put on the development of behavioral models to predict the nonlinear behavior of RF transmitters and to compensate them. Many behavioral models for SISO RF transmitters have been proposed in the literature e.g., Parallel Hammerstein (PH) [36, 37], generalized memory polynomial (GMP) [18, 38], vector-switched memory polynomial [39] and truncated Volterra models [40–42]. These developed models are reduced forms of the general Volterra series. Therefore, the Volterra series represents a mature technique for modeling and compensating the nonlinear SISO systems.

Recently the research focus of industry and academia is directed to the development of multi-channel RF transmitters e.g., MIMO [43, 44] and concurrent multi-band [45, 46] as they are used to improve transmitter diversity. For SISO systems, behavioral models were developed based upon Volterra series. In order to develop behavioral models for multi-channel RF systems, it is natural to also start with the general Volterra series. In this chapter a time and complex base-band domain 2×2 MIMO Volterra model is presented.

2.1 Time domain MIMO Volterra

In order to highlight the difference between the nonlinear dynamic behavior of a SISO and MIMO system we first briefly outline the SISO Volterra theory. Let us assume a SISO nonlinear dynamic system whose input and output relationship can be represented as

$$y(t) = f(x(t)), \tag{2.1}$$

where $f(\cdot)$ is a nonlinear dynamic transfer function and $x(t)$, $y(t)$ are the input output signals, respectively. The SISO Volterra series for modeling nonlinear dynamic transfer function $f(\cdot)$ is [13]

$$y(t) = \sum_{p=0}^{\infty} \int_{-\infty}^{\infty} \dots \int_{-\infty}^{\infty} h_p(\tau_1, \dots \tau_n) x(t-\tau_1) \dots x(t-\tau_p) d\tau_1 \dots d\tau_p, \tag{2.2}$$

where h_p are the real-valued Volterra kernels of nonlinear order p.

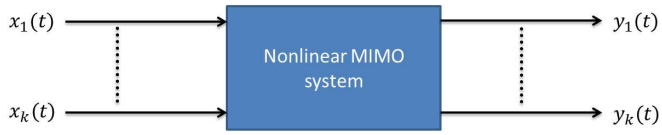

Figure 2.1: Nonlinear MIMO system.

Figure 2.1 shows a nonlinear MIMO system, the input-output relationship of a nonlinear MIMO system can be represented as

$$y_j(t) = f_j(x_1(t), \dots, x_k(t)) \quad j \in [1 \dots k]. \tag{2.3}$$

In (2.3), $f_j(\cdot)$ operates simultaneously on the input signals, indicating that the nonlinear behavior of a MIMO system is different from the SISO system. The $f_j(\cdot)$ can be modeled by the time domain MIMO Volterra series. An $M \times M$ MIMO system can be written as M MISO systems, the output of channel 1 of a 2×2

MIMO system can be written as [31]

$$y_1(t) = \int_{-\infty}^{\infty} h_{(1,1,1)}(\tau)x_1(t-\tau)d\tau + \int_{-\infty}^{\infty} h_{(1,1,2)}(\tau)x_2(t-\tau)d\tau \tag{2.4a}$$

$$+ \int_{-\infty}^{\infty}\int_{-\infty}^{\infty}\int_{-\infty}^{\infty} h_{(3,1,111)}(\tau_1,\tau_2,\tau_3)x_1(t-\tau_1)x_1(t-\tau_2)x_1(t-\tau_3)d\tau_1 d\tau_2 d\tau_3 \tag{2.4b}$$

$$+ \int_{-\infty}^{\infty}\int_{-\infty}^{\infty}\int_{-\infty}^{\infty} h_{(3,1,222)}(\tau_1,\tau_2,\tau_3)x_2(t-\tau_1)x_2(t-\tau_2)x_2(t-\tau_3)d\tau_1 d\tau_2 d\tau_3 \tag{2.4c}$$

$$+ \int_{-\infty}^{\infty}\int_{-\infty}^{\infty}\int_{-\infty}^{\infty} h_{(3,1,112)}(\tau_1,\tau_2,\tau_3)x_1(t-\tau_1)x_1(t-\tau_2)x_2(t-\tau_3)d\tau_1 d\tau_2 d\tau_3 \tag{2.4d}$$

$$+ \int_{-\infty}^{\infty}\int_{-\infty}^{\infty}\int_{-\infty}^{\infty} h_{(3,1,122)}(\tau_1,\tau_2,\tau_3)x_1(t-\tau_1)x_2(t-\tau_2)x_2(t-\tau_3)d\tau_1 d\tau_2 d\tau_3 \tag{2.4e}$$

$$+ \ldots + \int_{-\infty}^{\infty}\ldots\int_{-\infty}^{\infty} h_{(p,1,11\ldots1)}(\tau_1,\ldots,\tau_p)x_1(t-\tau_1)\ldots x_1(t-\tau_p)d\tau_1\ldots d\tau_p \tag{2.4f}$$

$$+ \ldots$$

where $h_{(nonlinear\,order, output\,channel, input\,combination)}$ indicates real-value MIMO Volterra kernels for a specific nonlinear order, output channel and input signal(s) combination. In (2.4a), $h_{(1,1,1)}$ and $h_{(1,1,2)}$ are the linear kernels of the input signals $x_1(t)$ and $x_2(t)$, respectively. In (2.4b) and (2.4c), $h_{(3,1,111)}$, $h_{(3,1,222)}$ represent 3^{rd} order self-kernels, whereas $h_{(3,1,112)}$, $h_{(3,1,122)}$ in (2.4d) and (2.4e), respectively, are the cross-kernels. These cross-kernels are due the coupling of signals from one channel to another. $h_{(p,1,11\ldots1)}$ in (2.4f) is the p-th order self-kernel.

The self-kernels have the same symmetry properties as the SISO Volterra kernels, i.e., $h_{(3,1,111)}(\tau_1,\tau_2,\tau_3) = h_{(3,1,111)}(\tau_2,\tau_1,\tau_3)$ for all the permutation of τ_1, τ_2 and τ_3. However, the cross-kernels have lower symmetry compared to the self-kernels [31], e.g., $h_{(3,1,112)}(\tau_1,\tau_2,\tau_3) = h_{(3,1,112)}(\tau_2,\tau_1,\tau_3)$ only for the permutation of τ_1, τ_2, but not for other permutation of τ_1, τ_2, τ_3, i.e., $h_{(3,1,112)}(\tau_1,\tau_2,\tau_3) \neq h_{(3,1,112)}(\tau_1,\tau_3,\tau_2)$. Similarly $h_{(3,1,122)}(\tau_1,\tau_2,\tau_3) = h_{(3,1,122)}(\tau_1,\tau_3,\tau_2)$ for the permutation of τ_2, τ_3 but not for the other permutation of τ_1, τ_2 and τ_3.

2.2 Complex base-band MIMO Volterra

In wireless communication systems, the input-output signals are represented on complex base-band form as the bandwidth of the signal is in the order of kHz to MHz, while the operational carrier frequency is typically in the order of GHz. Since

the primary interest is the frequencies close to the carrier frequency. A common method to represent a signal close to the carrier is to use a complex valued base-band signal [47]. The complex base-band discrete time SISO Volterra model is [38]

$$y(n) = \sum_{p=1}^{P} \sum_{m_1=0}^{M} \cdots \sum_{m_p=m_{p-1}}^{M} \sum_{m_{p+1}=0}^{M} \cdots \sum_{m_{2p-1}=m_{2p-2}} h_{2p-1}(m_1, \ldots, m_{2p-1}) \times x(n-m_1) \ldots x(n-m_p) x(n-m_{p+1})^* \ldots x(n-m_{2p-1})^*, \tag{2.5}$$

where $x(n)$,$y(n)$ are n^{th} samples of the complex base-band input and output signals, respectively, h_p is the complex-valued p^{th} order kernel, and $(\cdot)^*$ represents the complex conjugate. In (2.5), $h_3(m_1, m_2, m_3) = h_3(m_2, m_1, m_3)$ due to kernel symmetry, thus the redundant terms are removed. Moreover, even-order kernels are also removed since their effect can be omitted in band-limited modeling [15]. We extend the model in (2.5) to the MIMO case. The output signal is then

$$y_1(n) = \sum_{m=0}^{M} h_{(1,1,1)}(m) x_1(n-m) + \sum_{m=0}^{M} h_{(1,1,2)}(m) x_2(n-m) \tag{2.6a}$$

$$+ \sum_{m_1=0}^{M} \sum_{m_2=m_1}^{M} \sum_{m_3=0}^{M} h_{(3,1,111)}(m_1, m_2, m_3) x_1(n-m_1) x_1(n-m_2) x_1^*(n-m_3) \tag{2.6b}$$

$$+ \sum_{m_1=0}^{M} \sum_{m_2=m_1}^{M} \sum_{m_3=0}^{M} h_{(3,1,222)}(m_1, m_2, m_3) x_2(n-m_1) x_2(n-m_2) x_2^*(n-m_3) \tag{2.6c}$$

$$+ \sum_{m_1=0}^{M} \sum_{m_2=m_1}^{M} \sum_{m_3=0}^{M} h_{(3,1,112)}(m_1, m_2, m_3) x_1(n-m_1) x_1(n-m_2) x_2^*(n-m_3) \tag{2.6d}$$

$$+ \sum_{m_1=0}^{M} \sum_{m_2=m_1}^{M} \sum_{m_3=0}^{M} h_{(3,1,221)}(m_1, m_2, m_3) x_2(n-m_1) x_2(n-m_2) x_1^*(n-m_3) \tag{2.6e}$$

$$+ \sum_{m_1=0}^{M} \sum_{m_2=0}^{M} \sum_{m_3=0}^{M} h_{(3,1,121)}(m_1, m_2, m_3) x_1(n-m_1) x_2(n-m_2) x_1^*(n-m_3) \tag{2.6f}$$

$$+ \sum_{m_1=0}^{M} \sum_{m_2=0}^{M} \sum_{m_3=0}^{M} h_{(3,1,122)}(m_1, m_2, m_3) x_1(n-m_1) x_2(n-m_2) x_2^*(n-m_3) \tag{2.6g}$$

$$+ \ldots$$

In (2.6), $y_1(n)$ is the output signal of channel 1, $x_1(n)$ and $x_2(n)$ are the complex base-band input signals. Equation (2.6a) represents linear kernels, one for each

input signals. Self-kernels are represented in (2.6b) and (2.6c); these self-kernels have the same symmetry properties as the SISO Volterra series. Cross-kernels given by (2.6d) and (2.6e) have the same symmetry properties as (2.4d) and (2.4e) i.e., $h_{(3,1,112)}(m_1, m_2, m_3) = h_{(3,1,112)}(m_2, m_1, m_3)$ but not for other permutations of m_1, m_2 and m_3. Cross-kernels given in (2.6f) and (2.6g) do not have any symmetry properties for any permutations of m_1, m_2 and m_3. Furthermore, kernels given in (2.6f) and (2.6g) are not present in a continuous time domain MIMO Volterra model.

2.3 Nonlinear and linear cross-talk in MIMO transmitter

In electrical systems, coupling or cross-talk effect is due the interference of a signal from one or more sources. In MIMO transmitters, cross-talk occurs due the interference between the signals of different channels. In most cases these signals have the same operational frequency and transmission power. Therefore, cross-talk is likely to occur and is difficult to avoid entirely, especially in an integrated circuit design where the size is important.

In a MIMO transmitter, cross-talk can be categorized as input (nonlinear) and output (linear) cross-talk, depending whether the cross-talk occurs before or after the nonlinear component [28] i.e., the PA, as shown in Figure 2.2. In Figure 2.2, α and β are the impulse response of the linear filters before and after the PAs, indicating the amount of cross-talk. In this thesis, the cross-talk is assumed to be frequency independent i.e., memory less. Note that in the rest of the thesis, input cross-talk will be referred as nonlinear cross-talk and output cross-talk as linear cross-talk [27].

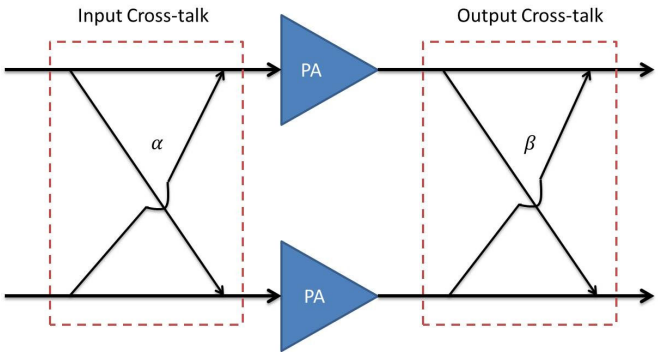

Figure 2.2: 2×2 RF MIMO transmitter, α and β represents input and output cross-talk, respectively.

The input-output relationship of a 2×2 MIMO transmitter in presence of non-

linear cross-talk can be represented as

$$\begin{aligned} y_1 &= f_1(x_1(n)\,,\, \alpha \star x_2(n)) \\ y_2 &= f_2(\alpha \star x_1(n)\,,\, x_2(n)), \end{aligned} \tag{2.7}$$

where α is the amount of cross-talk at the input of the PAs and $\star$ indicates convolution. In (2.7), $f_1(\cdot)$ and $f_2(\cdot)$ are the nonlinear dynamic transfer functions of channel 1 and 2, respectively. These nonlinear transfer functions can be modeled by (2.6) since $f_1(\cdot)$ and $f_2(\cdot)$ operate simultaneously on both input signals. In the presence of linear cross-talk, the output of a 2×2 MIMO transmitter can represented as

$$\begin{aligned} y_1 &= f_1(x_1(n)) + \beta \star f_2(x_2(n)) \\ y_2 &= \beta \star f_1(x_1(n)) + f_2(x_2(n)). \end{aligned} \tag{2.8}$$

where β is the amount of cross-talk at the output of the PAs. Equation (2.8) indicates that the output of each channel is a linear combination of $f_1(\cdot)$ and $f_2(\cdot)$, respectively, which can be modeled by the SISO Volterra series given in (2.5). In presence of no cross-talk i.e., α and β are equal two zero, Figure 2.2 can be viewed as two separate SISO systems and the output of each channel can be modeled by (2.5).

Note that the models discussed in this thesis do not require the prior knowledge of the particular cross-talk effect or cross-talk type, i.e., the cross-talk is not an input parameter to these models. In the system identification, the model parameters take into account the amount of cross-talk. Moreover, any mismatch in the level of cross-talk will also be taken into account by the model parameters during system identification.

2.4 System Identification

In order to estimate the model parameters, the output signal model of a 2×2 MIMO PA can be written as

$$\begin{bmatrix} \mathbf{y}_1 \\ \mathbf{y}_2 \end{bmatrix} = \begin{bmatrix} \mathbf{H}_1 & 0 \\ 0 & \mathbf{H}_2 \end{bmatrix} \begin{bmatrix} \theta_1 \\ \theta_2 \end{bmatrix} + \begin{bmatrix} \mathbf{v}_1 \\ \mathbf{v}_2 \end{bmatrix}, \tag{2.9}$$

where $\mathbf{H}_1$ and $\mathbf{H}_2$ are the regression matrices for channel 1 and 2, respectively. The signals $\mathbf{v}_1(n)$ and $\mathbf{v}_2(n)$ are uncorrelated white gaussian noise with zero-mean, θ_1 and θ_2 are the complex valued parameter vectors. Note that the outputs are decoupled in (2.9), i.e., the parameters for channel 1 and 2 are independently estimated. The regression matrix H_1 is

$$\mathbf{H}_1 = \begin{bmatrix} \phi_1(1) & \phi_2(1) & \dots & \phi_O(1) \\ \phi_1(2) & \phi_2(2) & \dots & \phi_O(2) \\ \vdots & \vdots & \ddots & \vdots \\ \phi_1(N) & \phi_2(N) & \dots & \phi_O(N) \end{bmatrix}, \tag{2.10}$$

where $\phi_i(\cdot)$ are the basis functions of the model. In (2.10), O is the total number of basis functions and N is the number of samples.

The 2×2 Volterra model in (2.6) is linear in the parameters. A linear least square estimation (LSE) [48] can be used to estimate the model parameters by minimizing the cost function

$$\hat{\theta}_j = \arg\min_{\theta_j} \|\mathbf{y}_j - \mathbf{H}_j\theta_j\|. \;\; j \in [1,2] \tag{2.11}$$

The parameters, θ_j, in (2.11) can be determined as

$$\hat{\theta}_j = (\mathbf{H}_j^*\mathbf{H}_j)^{-1}\mathbf{H}_j^*\mathbf{y}_j, \tag{2.12}$$

where $\hat{\theta}_j$ are the estimated parameters. Equation (2.9) can also be used for modeling concurrent dual-band PAs where the input and output signals are operating at different carrier frequencies. In papers **A**, **B** and **C**, LSE is employed to identify the model parameters. Note that in all experiments, noise is assumed to be zero-mean white gaussian noise (WGN) which results in unbiased estimates using LSE. However, in case of non zero-mean WGN, LSE will result in biased estimates [49, 50].

Chapter 3

Experimental Setup

This chapter gives a brief introduction to the experimental setups and performance metrics used in papers **A**, **B** and **C**. The experimental setups used in papers **A** and **B** are described in Section 3.1, whereas the experimental setup used in paper **C** is described in Section 3.2.

3.1 MIMO PA experimental setup

The experimental setup used to obtain the data needed for modeling and DPD of the 2×2 MIMO PA in paper **A** is shown in Figure 3.1. The test signals were

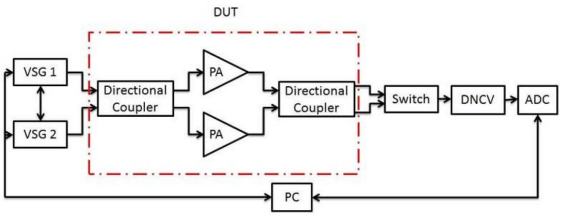

Figure 3.1: Experimental setup used in paper **A**. The DUT consists of two Mini-Circuit ZVE-8G+ amplifier sandwich between the directional couplers.

generated using two Rhode & Schwarz (R&S) SMBV 100a vector signal-generators (VSGs) connected in master-slave configurations and were base-band synchronized. RF coherency was achieved by feeding a common local oscillator (LO) signal to the VSGs. The LO signal was generated using Holzworth HS9003A RF synthesizer. To study the effect of partially non-coherent RF signals on the performance of DPD algorithm, the VSGs were only sharing a common 10 MHz reference clock and the common LO was removed. The signals were operating at a carrier frequency of 2.14 GHz and were down-converted to IF using a wide-band down-converter. The IF signals were digitized using SP-devices ADQ-214 analog-to-digital converter (ADC)

which has a resolution of 14-bits and the maximum sampling rate is 400 MHz. The total digital bandwidth achievable with the ADC is 200 MHz.

Experimental setup used in paper **B** was the same as in **A** except the receiver which consists of two down-conversion chain formed with 2 mixers and band-pass filters. Moreover, the carrier frequency was 1.8 GHz and −20-dB cross-talk level was used at the input and output of the DUT, whereas in paper **A**, two cross-talk levels were used, namely, −20 and −30-dB.

3.2 Concurrent dual-band PA setup

The experimental setup used in paper **C** is shown in Figure 3.2. Two R&S SMBV 100a VSGs were used to generate two two-tone signals operating at the carrier frequencies of 2 and 2.3 GHz concurrently. The RF signals were combined using a wide-band power combiner. The output RF signal from the DUT was down-converted to an IF signal using a wide-band down-converter. Since the output RF signal has two operational carrier frequencies, the LO frequency of the down-converter was tuned for down-converting the lower and/or upper band signal one at a time. The down-converted signal was digitized using the above mentioned ADC. The VSGs were base-band synchronized. Coherent RF signals were generated using two external LO signals. The LO signals were generated using the Holzworth HS9003A RF synthesizer.

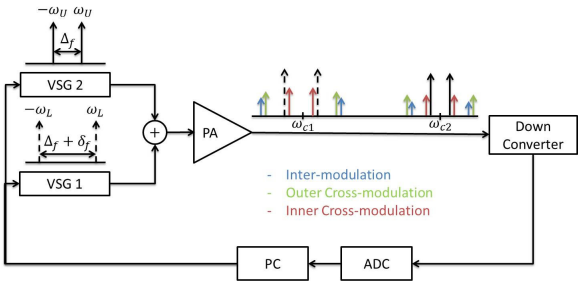

Figure 3.2: Measurement setup used in paper **B**.

3.3 Coherent averaging

To improve the performance of the measurement system, coherent averaging was performed to increase the dynamic range of the system. In coherent averaging, repetitive signals are used as an input to the DUT and the sampling frequency and number of samples of the measured signals are chosen such that an integer number of repeated periods are captured and arithmetic averaging is performed [51]. Coherent averaging can reduce the effect of measurement noise by $20log_{10}(N)$, where N is the integer number of measurements.

3.4 Devices Under Test

In paper **A** and paper **B**, the DUT consists of two Mini-Circuit ZVE-8G+ general purpose wide-band amplifiers sandwiched between two directional couplers. The PA has a nominal small signal gain of 30 dB and the output 1 dB compression point of 32 dBm. In paper **C**, two PAs were used as the DUTs namely ZVE-8G+ and a free-scale MRF 521120 HS Doherty PA with a typical gain of 15 dB. The DUTs used in papers **A**, **B** and **C** were warmed up for an hour, and then operated at steady stage. The assumption of a time invariant system should, hence, be valid.

3.5 Experimental signals

In paper **A**, two different sets of WCDMA signals were used for the identification and validation of the proposed models. Each set consisted of two different WCDMA signals for each channel. The sampling rate of the signals was 30.72 MHz and the total number of samples was 40960 with peak-to-average power ratio (PAPR) of more than 8 dB. In paper **B**, multi-tone signals with a bandwidth of 4.8 MHz were used to evaluate the performance of the sparse DPD model. The total number of samples used were 20000 and at a sampling rate of 80 MHz with PAPR of more than 9 dB.

In paper **C**, two two-tone signals were used. To study the memory effects of a concurrent dual-band PA, these signals were swept both in power and frequency.

3.6 Performance Metrics

In order to evaluate the performances of the proposed models, the metrics used are described below.

- Normalized mean-square error (NMSE) is used in paper **A** and **B**, respectively, and is defined as [8]

$$\text{NMSE} = \frac{\int \Phi_e(f)\, df}{\int \Phi_y(f)\, df}, \tag{3.1}$$

  where $\Phi_e(f)$ is the error power spectrum and $\Phi_y(f)$ is the power spectrum of the measured output signal; integration is carried out across the available bandwidth.

- Adjacent channel error power ratio (ACEPR) is used only in paper **A** and is defined as [8]

$$\text{ACEPR} = \frac{\int_{\text{adj. ch.}} \Phi_e(f)\, df}{\int_{\text{ch.}} \Phi_y(f)\, df}, \tag{3.2}$$

  where the integration in the numerator is performed over the adjacent channel with maximum error power and in the denominator, integration is performed over the input channel.

- Adjacent channel power ratio (ACPR) is used in paper **A** and **B**, respectively, and is defined as [8]

$$\text{ACPR} = \frac{\int_{\text{adj. ch.}} \Phi_y(f)\, df}{\int_{\text{ch.}} \Phi_y(f)\, df}, \tag{3.3}$$

  where in the numerator integration is performed over the adjacent channel with the largest amount of power; in the denominator, integration is performed over the input channel band.

To evaluate the frequency dependency in paper **C**, 3-D asymmetric energy surfaces were plotted by subtracting the upper intermodulation (IM) and cross-modulation (CM) products from their corresponding lower IM and CM products, respectively. As such the amount of asymmetry between the IM and CM products, respectively can be determined. The asymmetry between the IM products can be defined as [52]

$$\text{IM}_{asymmetry} = 20 \times \log_{10}(\frac{IM_U}{IM_L}) = IM_{U_{dB}} - IM_{L_{dB}}, \tag{3.4}$$

where IM_U and IM_L indicates upper and lower IM products. The classical 2-D plots for both frequency and input power sweep were also used. Furthermore, for the power sweep, the measured IM and CM amplitudes were also evaluated against a 3:1 amplitude slope. The 3:1 amplitude slope indicates whether or not the amplitudes of IM and CM products are proportional to the third power of the input amplitude [53].

Chapter 4

Behavioral Modeling, Linearization and Parameter Reduction in 2×2 MIMO Power Amplifier

This chapter presents three behavioral models for modeling the 2×2 MIMO transmitters described in paper **A** in presence of different types of cross-talk. The relationship between DUT and its DPD structure for different types of cross-talk is also discussed. Moreover, depending upon the type of cross-talk, the correct model for sufficient DPD performance in terms of NMSE and ACPR is also highlighted. A comparative study has also been made with a previously published 2×2 PH model [28].

Parameter reduction techniques are important tools in system analysis. Especially, the behavioral models (DPD models) for a multi-channel transmitter suffer from a large number of model parameters, thus making it difficult to identify the most significant model parameters. The parameter reduction technique presented in paper **B** is also discussed briefly, where the least-absolute shrinkage and selection operator (LASSO) algorithm is implemented to have a working sparse MIMO Volterra model for DPD.

4.1 Generalized memory polynomial models for a 2×2 MIMO amplifier

Figure 3.1 shows the measurement setup used in paper **A**. Three cross-talk effects were studied, namely nonlinear cross-talk (input cross-talk), linear cross-talk (output cross-talk) and nonlinear & linear cross-talk (input and output cross-talk). To introduce linear cross-talk only, directional couplers at the output of the PA are used and the output can be represented as in (2.8). The nonlinear functions, $f_1(\cdot)$ and $f_2(\cdot)$ in (2.8) can be modeled by the SISO generalized memory polynomial (GMP). The GMP model was used as it is based on physical knowledge of PAs [38] and

has been extensively studied for both behavioral modeling and DPD [38, 54]. The resulting model is a generalized memory polynomial for linear cross-talk (GMPLC)

$$\begin{aligned} y_i(n) = &\sum_{p=1}^{P}\sum_{m_1=0}^{M_1}\sum_{m_2=0}^{M_2} g_{i_{p,(m_1,m_2)}} x_i(n-m_1)|x_i(n-m_1-m_2)|^{2(p-1)} + \\ &\sum_{p=1}^{P}\sum_{m_1=0}^{M_1}\sum_{m_2=0}^{M_2} g_{j_{p,(m_1,m_2)}} x_j(n-m_1)|x_j(n-m_1-m_2)|^{2(p-1)}, \\ &\qquad\qquad i \neq j,\ i,j \in [1,2] \end{aligned} \tag{4.1}$$

where $g_{i_{p,(m_1,m_2)}}$ are complex-value model parameters, P is the nonlinear order, and M_1 and M_2 are the memory depths.

In presence of nonlinear cross-talk only, the output of the 2×2 MIMO PA is defined by (2.7), where $f_1(\cdot)$ and $f_2(\cdot)$ operates simultaneously on both input signals. To compensate for such effects, the model should include cross-terms between x_1 and x_2 along with nonlinear SISO combinations given by (4.1). By combining nonlinear cross-talk with the SISO GMP model, the resulting models are the extended generalized memory polynomial for nonlinear cross-talk (EGMPNLC) and generalized memory polynomial for nonlinear cross-talk (GMPNLC) models. The difference between EGMPNLC and GMPNLC is that the former contains more cross-kernels. The GMPNLC model is defined as

$$\begin{aligned} y_i(n) = &\sum_{p=1}^{P}\sum_{q=1}^{P-p+1}\sum_{m_1=0}^{M_1}\sum_{m_2=0}^{M_2} g_{i,p,q,(m_1,m_2)} x_i(n-m_1) \\ &|x_i(n-m_1-m_2)|^{2(p-1)}|x_j(n-m_1-m_2)|^{2(q-1)} + \\ &\sum_{p=1}^{P}\sum_{q=1}^{P-p+1}\sum_{m_1=0}^{M_1}\sum_{m_2=0}^{M_2} g_{j,p,q,(m_1,m_2)} x_j(n-m_1) \\ &|x_j(n-m_1-m_2)|^{2(p-1)}|x_i(n-m_1-m_2)|^{2(q-1)}. \end{aligned} \tag{4.2}$$

The EGMPNLC model is defined as in Table 4.1. The EGMPNLC terms shown in Table 4.1 for 3^{rd} order nonlinearity ($NL = 3$) are equal to the 3^{rd} order terms in the complex base-band MIMO Volterra. If $m_2 = m_3$, (2.6b) - (2.6e) correspond to the terms in rows 1, 4, 6, 2, and 8 in Table 4.1 except for the terms in row 3 and 7 which correspond to (2.6f) and (2.6e), respectively, if $m_1 = m_3$. Therefore, the EGMPNLC model is a subset of the nonlinear MIMO Volterra model, similarly GMPLC ⊂ GMPNLC ⊂ EGMPNLC, where ⊂ denotes subset.

Note that in presence of both linear and nonlinear cross-talk, the output signals of the MIMO PA will contain both SISO nonlinear terms and the cross-terms. Therefore, EGMPNLC and GMPNLC can model such behavior, since they include both self and cross-kernels.

Table 4.1: Basis functions of the EGMPNLC models, where $L_1 = (n - m_1)$, $L_2 = (n - m_1 - m_2)$ and NL is the order of nonlinearity.

$NL = 1$	$NL = 3$	$NL = 5$	$\cdots$	$NL = \infty$
$x_1(L_1)$	$x_1(L_1)\lvert x_1(L_2)\rvert^2$	$x_1(L_1)\lvert x_1(L_2)\rvert^4$	$\cdots$	$x_1(L_1)\lvert x_1(L_2)\rvert^{(NL-1)}$
$x_2(L_1)$	$x_1(L_1)\lvert x_2(L_2)\rvert^2$	$x_1(L_1)\lvert x_2(L_2)\rvert^4$	$\cdots$	$x_1(L_1)\lvert x_2(L_2)\rvert^{(NL-1)}$
	$x_2(L_1)\lvert x_1(L_2)\rvert^2$	$x_2(L_1)\lvert x_1(L_2)\rvert^4$	$\cdots$	$x_2(L_1)\lvert x_1(L_2)\rvert^{(NL-1)}$
	$x_2(L_1)\lvert x_2(L_2)\rvert^2$	$x_2(L_1)\lvert x_2(L_2)\rvert^4$	$\cdots$	$x_2(L_1)\lvert x_2(L_2)\rvert^{(NL-1)}$
	$x_1(L_1)x_1(L_2)x_2^*(L_2)$	$x_1(L_1)\lvert x_1(L_2)\rvert^2x_1(L_2)x_2^*(L_2)$	$\cdots$	$x_1(L_1)\lvert x_1(L_2)\rvert^{(NL-3)}x_1(L_2)x_2^*(L_2)$
	$x_1(L_1)x_1^*(L_2)x_2(L_2)$	$x_1(L_1)\lvert x_1(L_2)\rvert^2x_1^*(L_2)x_2(L_2)$	$\cdots$	$x_1(L_1)\lvert x_1(L_2)\rvert^{(NL-3)}x_1^*(L_2)x_2(L_2)$
	$x_2(L_1)x_1(L_2)x_2^*(L_2)$	$x_1(L_1)\lvert x_2(L_2)\rvert^2x_1(L_2)x_2^*(L_2)$	$\cdots$	$x_1(L_1)\lvert x_2(L_2)\rvert^{(NL-3)}x_1(L_2)x_2^*(L_2)$
	$x_2(L_1)x_1^*(L_2)x_2(L_2)$	$x_1(L_1)\lvert x_2(L_2)\rvert^2x_1^*(L_2)x_2(L_2)$	$\cdots$	$x_1(L_1)\lvert x_2(L_2)\rvert^{(NL-3)}x_1^*(L_2)x_2(L_2)$
		$x_1(L_1)\lvert x_1(L_2)\rvert^2\lvert x_2(L_2)\rvert^2$	$\cdots$	$x_1(L_1)\lvert x_1(L_2)\rvert^{(NL-1)/2}\lvert x_2(L_2)\rvert^{(NL-1)/2}$
		$x_2(L_1)\lvert x_1(L_2)\rvert^2\lvert x_2(L_2)\rvert^2$	$\cdots$	$x_2(L_1)\lvert x_1(L_2)\rvert^{(NL-1)/2}\lvert x_2(L_2)\rvert^{(NL-1)/2}$
		$x_2(L_1)\lvert x_1(L_2)\rvert^2x_1(L_2)x_2^*(L_2)$	$\cdots$	$x_2(L_1)\lvert x_1(L_2)\rvert^{(NL-3)}x_1(L_2)x_2^*(L_2)$
		$x_2(L_1)\lvert x_1(L_2)\rvert^2x_1^*(L_2)x_2(L_2)$	$\cdots$	$x_2(L_1)\lvert x_1(L_2)\rvert^{(NL-3)}x_1^*(L_2)x_2(L_2)$
		$x_2(L_1)\lvert x_2(L_2)\rvert^2x_1(L_2)x_2^*(L_2)$	$\cdots$	$x_2(L_1)\lvert x_2(L_2)\rvert^{(NL-3)}x_1(L_2)x_2^*(L_2)$
		$x_2(L_1)\lvert x_2(L_2)\rvert^2x_1^*(L_2)x_2(L_2)$	$\cdots$	$x_2(L_1)\lvert x_2(L_2)\rvert^{(NL-3)}x_1^*(L_2)x_2(L_2)$

4.2 Behavioral Modeling results

Table 4.2 summarizes the performance of each model in terms of NMSE and ACEPR. In the presence of linear cross-talk only, all models resulted in an NMSE of approximately −50 dB, whereas in terms of ACEPR, the GMPLC model resulted in an ACEPR of −58.9 dB which is 0.3 and 1.3 dB lower in performance than GMPNLC and EGMPNLC, respectively. For the cases of nonlinear and nonlinear & linear cross-talk, GMPNLC resulted in the same performance and is 5 dB lower in performance than EGMPNLC in NMSE and 2 dB in ACEPR. In presence of nonlinear and nonlinear & linear, previously published 2×2 PH model has inferior performance compared to GMPNLC and EGMPNLC in terms of NMSE and ACEPR.

Table 4.2: NMSE/ACEPR [dB] for given behavioral models and cross-talk type, the cross-talk level was -20 dB.

Model	Linear NMSE/ACEPR	Nonlinear NMSE/ACEPR	Nonlinear&Linear NMSE/ACEPR	No of coeff
2×2 PH	-41.5/-56.6	-40.1/-54.7	-40/-54.3	180
GMPLC	-50.1/-58.9	-42.3/-52.7	-40,1/-51.9	126
GMPNLC	-50.3/-59.2	-45.4/-58.9	-45.1/-58.3	242
EGMPNLC	-50.2/-60.2	-50.4/-60.1	-50.3/-60.3	486

As shown in Table 4.2, to model a DUT with linear cross-talk, the GMPLC model can be used since it gives approximately the same model performance compare to GMPNLC and EGMPNLC models with less number of model parameters. In the presence of nonlinear and nonlinear & linear cross-talk, the DUT can be modeled by GMPNLC and EGMPNLC models with results in higher model performance compared to GMPLC model in terms of NMSE and ACEPR. Moreover, the results in Table 4.2 illustrate that 2×2 PH model is not an adequate model for the MIMO PA, even in the presence of linear cross-talk the model error is higher compared to the proposed models.

4.3 Linearization results

In an indirect learning architecture (ILA), a post-inverse of the DUT is identified and used as a pre-inverse (DPD). Moreover, if the post-inverse is modeled by a memory polynomial e.g., GMPLC, the input and output are interchanged [32]. Figure 4.1 show the relationship between the DUTs and their pre-inverse structures, and Table 4.3 summarize the model usage for behavioral modeling and DPD under different cross-talk conditions.

In the presence of nonlinear cross-talk, the corresponding DPD structure is shown in Figure 4.1 (a), where inverse nonlinear function $f^{-1}(\cdot)$ is followed by the

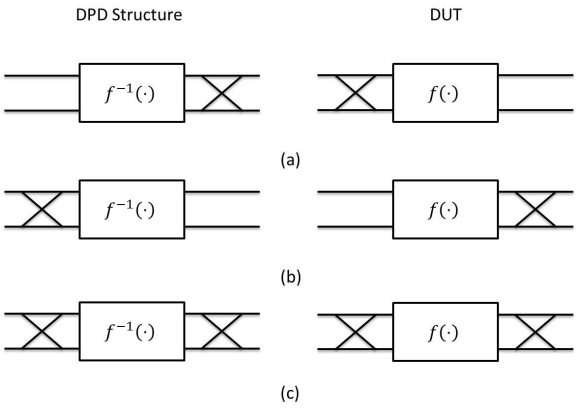

Figure 4.1: DUT and corresponding DPD structure

cross-talk. To linearize the DUT with nonlinear cross-talk, the DPD structure can be modeled by GMPLC. Figure 4.2 show the linearized output spectra of the DUT in presence of nonlinear cross-talk. The GMPLC model resulted in an NMSE and ACPR of approximately -45 and -58-dB, respectively, when used as an inverse model (DPD model). Figure 4.2 shows that EGMPNLC and GMPNLC gives the same performance as GMPLC, this is because these models also include the SISO nonlinear terms which are present in the GMPLC model. The 2×2 PH model resulted in an inferior performance which indicates that the model is not suitable for such PA. Moreover, Figure 4.2 suggest that GMPLC is an adequate DPD model for the DUT with nonlinear cross-talk.

In presence of linear cross-talk, the DUT has the structure of nonlinearity $f(\cdot)$ followed by the cross-talk. Therefore, by implementing ILA principle for DPD, the corresponding DPD structure is shown in 4.1 (b), i.e., cross-talk followed by $f^{-1}(\cdot)$. When used as an inverse model, GMPNLC and EGMPNLC models resulted in similar DPD performance with an NMSE and ACPR of approximately -45 and -58-dB. The GMPLC resulted in inferior performance due to lack of cross-terms required to model such DPD structure. The linearized output spectra of the DUT with linear cross-talk is shown in Figure 4.3.

In presence of both linear and nonlinear cross-talk, the corresponding DPD structure is shown in Figure 4.1 (c) which can be modeled by GMPNLC and EGMPNLC. The linearized output spectra is shown in 4.4.

Figure 4.5 shows the impact of coherent and partially non-coherent transmitter on the performance of DPD. For partially non-coherent signal generation, the DPD resulted in an NMSE and ACPR of -45.1 and -56.1-dB, whereas coherent measurement resulted in an NMSE and ACPR of -48.5 and -59.4-dB for channel 1 of a 2×2 MIMO PA when the coherent averaging was equal to 100. Figure 4.5 shows that even with the increase in number of averaging, the difference between coherent

Table 4.3: Summary of model usage for different cross-talk cases.

Model	Cross-talk type	Behavioral model performance	DPD performance
GMPLC	Linear	Sufficient	Not sufficient
GMPNLC		Sufficient	Sufficient
EGMPNLC		Sufficient	Sufficient
GMPLC	Nonlinear	Not sufficient	Sufficient
GMPNLC		Sufficient	Sufficient
EGMPNLC		Sufficient	Sufficient
GMPLC	Nonlinear&linear	Not sufficient	Not sufficient
GMPNLC		Sufficient	Sufficient
EGMPNLC		Sufficient	Sufficient

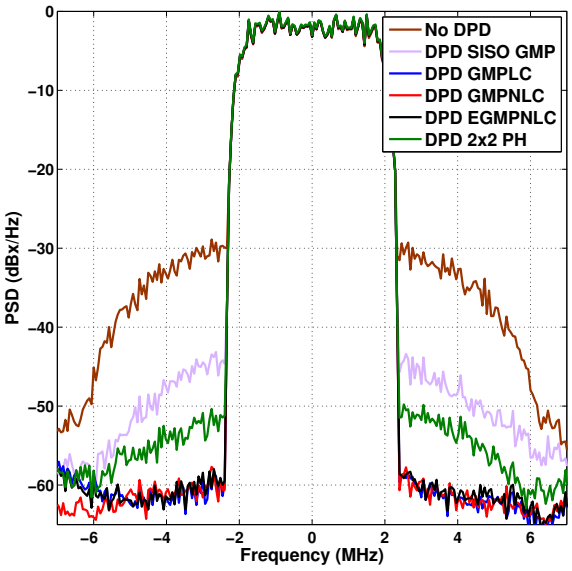

Figure 4.2: Linearized output of DUT in presence of nonlinear cross-talk

and partially non-coherent measurement on the performance of DPD is $2.5-3$ and $3-4$ dB in terms of NMSE and ACPR, respectively, depending upon additive noise level. These measurement results show that with partially non-coherent measurement i.e., when signal generators are not sharing the common LO and are just 10 MHz reference clock, the DPD performance degrades.

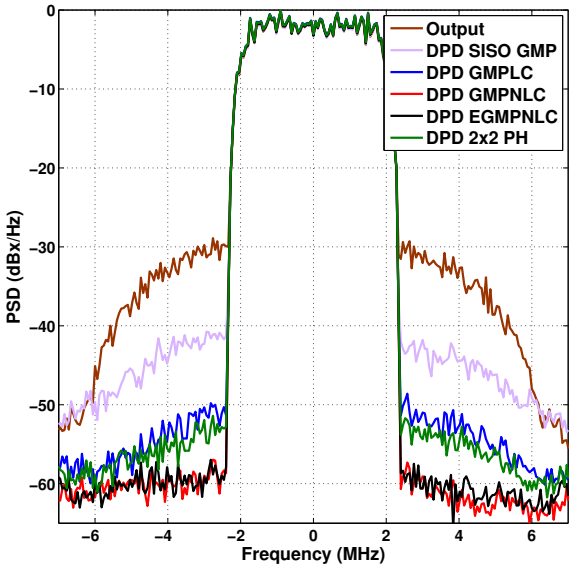

Figure 4.3: Linearized output of DUT in presence of linear cross-talk

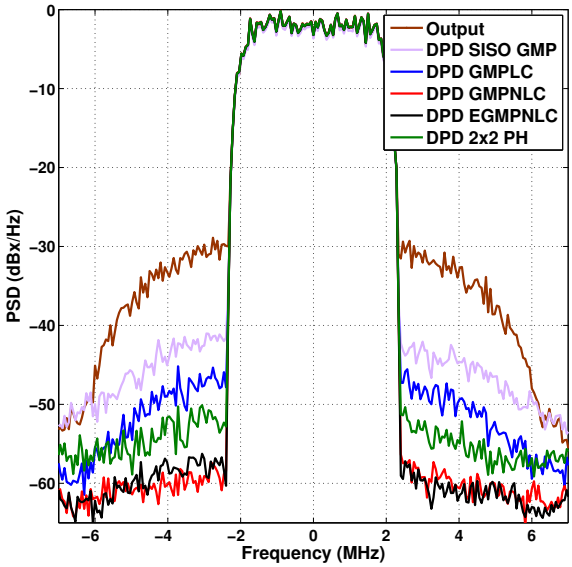

Figure 4.4: Linearized output of DUT in presence of nonlinear & linear cross-talk

4.4 Sparse estimation techniques

One particular problem associated with the generalization of SISO memory polynomial models to multiple input cases is the increase in the number of model param-

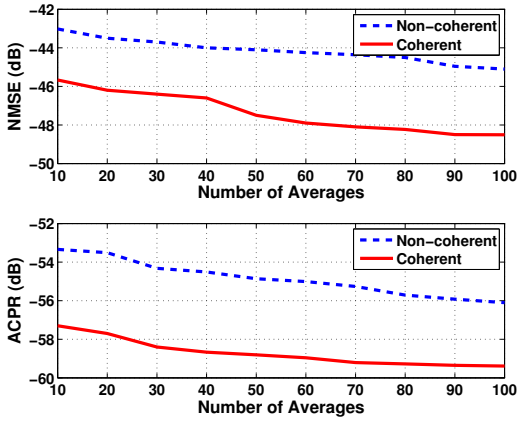

Figure 4.5: Measured NMSE and ACPR vs number of coherent averaging of the linearized output signal with coherent and partially non-coherent signal generation. The DUT had -30 dB nonlinear cross-talk and the inverse model for DPD was GMPNLC.

eters. The large number of parameters also has a negative effect in the LSE-based model identification (cf. (2.12)). First, the matrix inversion becomes computationally expensive, second, it raises numerical instability issues. Therefore, parameter reduction techniques are needed for MIMO and concurrent multi-band nonlinear systems.

Sparse estimation techniques are becoming popular since they enable to significantly reduce the number of model parameters required by behavioral modeling and DPD while achieving comparable performance in terms of both model performance and compensating distortions [55, 56]. Sparse estimation techniques and particularly LASSO are often used in biomedical applications for model selection [57, 58], where the number of basis functions are relatively high. LASSO seeks the most significant basis functions which then can be used to find model parameters that accurately represent the system behavior. The LASSO technique has previously been used for SISO behavioral modeling [59, 60]. The technique can also be implemented for MIMO and concurrent multi-band systems to reduce the number of parameters. The LASSO is given by

$$\begin{aligned} \underset{\{\boldsymbol{\theta}_j\}_j}{\text{minimize}} \quad & \sum_{j=1}^{K} \|\boldsymbol{x}_j - \mathbf{H}_j\boldsymbol{\theta}_j\|_2 \,, \\ \text{subject to} \quad & \sum_{n=1}^{N} R_n|\theta_j(n)| \leq \gamma_j. \end{aligned} \tag{4.3}$$

Table 4.4: MIMO predistorters performance with and without LASSO

Model	# of basis	NMSE	ACPR
2×2 MIMO Volterra	1402	-	-
2×2 sparse MIMO Volterra	220	-42 / -43 dB	-52 / -54 dB

In (4.3), $\|\cdot\|_2$ denotes the ℓ_2 norm, γ_j is the trade-off parameter for sparsity against model fitting, $\theta_j(n)$ is the n-th parameter of the vector $\boldsymbol{\theta}_j$. R_n is a scalar normalizing factor required since the model parameters have different scales of magnitude. R_n is set as the sample variance of the n-th column of the regression matrix $\mathbf{H}_j$. The problem in (4.3) can be solved using the convex solvers [61]. The basis functions are selected based upon there amplitude, i.e., the basis functions with lower amplitude than a certain value are not selected. Once the optimal basis functions are selected, LSE can be used to identify the sparse model parameters.

4.5 Sparse Volterra DPD Results

In paper **B**, the MIMO Volterra model defined in (2.6) was used as a DPD model for a 2×2 MIMO transmitter in the presence of -20 dB nonlinear & linear crosstalk. The initial sets of basis functions were 1402 found by using (2.6) with 9^{th} order nonlinearity and linear terms had a memory depth of 5. For 3^{rd}, 5^{th}, 7^{th} and 9^{th} order terms, the memory depths were 3, 2, 1 and 0. Table 4.4 summarizes the performance of the MIMO predistorters and Figure 4.6 shows the condition number of regression matrices when LSE was used with and without the implementation of the LASSO algorithm. The condition number of the Volterra system without LASSO is large which results in numerical instabilities, whereas, the reduced model has lower condition number which results in better numerical properties when LSE is used. Figure 4.7 shows the linearized output spectra of channel 1 and 2 of the MIMO PA.

Table 4.5 summarize the performance of GMPNLC model used as a behavioral model for modeling the nonlinear behavior of DUT in paper **B** with and without LASSO technique. In (4.2), the nonlinear order was 9 and memory depths M_1 and M_2 were 2 and 3, respectively. Such combinations of nonlinear order and memory depths resulted in 150 basis functions, whereas, when LASSO was implemented, the total number of model parameters reduced to 53 with comparable performance in terms of NMSE and ACEPR.

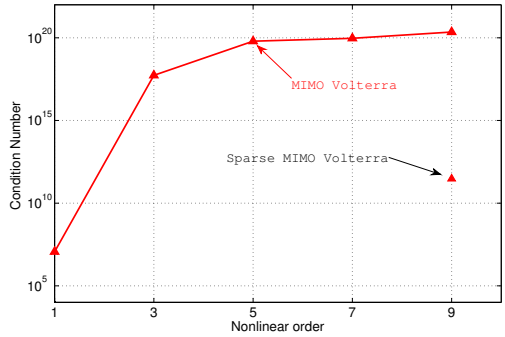

Figure 4.6: Condition number of the regression matrices with and without LASSO algorithm.

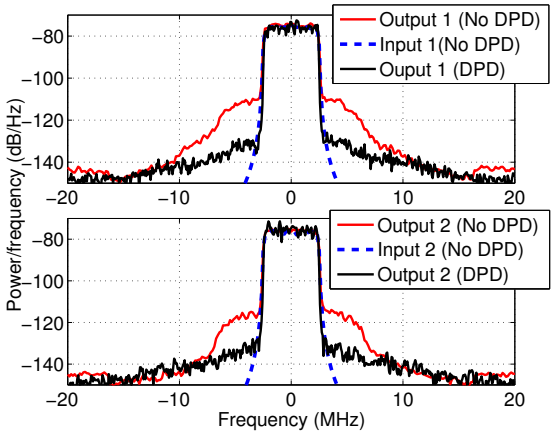

Figure 4.7: Linearized output spectra of 2×2 MIMO PA

Table 4.5: Performance of GMPNLC as behavioral model with LASSO algorithm for DUT in paper **B**

Model	# of basis	NMSE	ACEPR
GMPNLC	150	-45 / -44 dB	-56 / -55 dB
sparse GMPNLC	53	-44 / -43 dB	-54 /-54 dB

Chapter 5

Characterization of Memory Effects in Concurrent Dual-Band Power Amplifier

In wireless systems, RF PAs have traditionally been characterized using power swept continuous wave signals to measure amplitude-amplitude (AM/AM) and amplitude-phase (AM/PM) distortions. This is enough for narrow band systems such as a global system for mobile communications (GSM). For larger bandwidth system with fast changing signal envelope, the above technique is not enough [22]. Large research efforts have therefore been made to characterize the memory effects in RF PAs. Consequently, there are several techniques in which the nonlinear dynamic behavior of PA can be characterized. Among these techniques, the two-tone measurement technique is frequently used, where the signal is swept both in power and frequency. In a two-tone test, a signal operating at two frequencies is used to excite the DUT. In most cases, the 3^{rd} order intermodulation products (IM) amplitude and phase is used as a measure of nonlinearity. Metrics such as 1 dB compression point and 3^{rd} order intercept point are sometimes used to quantify the nonlinearity and are extracted from the measured IM products [62].

In a two-tone tests, the memory effects are also quantified from the measurement of frequency dependence and asymmetry of lower and upper IM products vs. tone spacing [22–26]. Sweeping the power of a two-tone signal and measuring the amplitudes of the IM products is sometimes used to identify sweet spots and the transition between large and small signal regimes of the DUT [63]. In [21], a 3^{rd} order Volterra kernel which is a function of three frequencies was found using three tone test signals and symmetry analysis of the 3^{rd} order Volterra kernel in the frequency domain was performed.

With the increasing interest for the development of multi-channel RF transmitters, methods for characterizing the memory effects become more important because of the presence of cross-terms as mentioned in chapter 2. In [64], a two

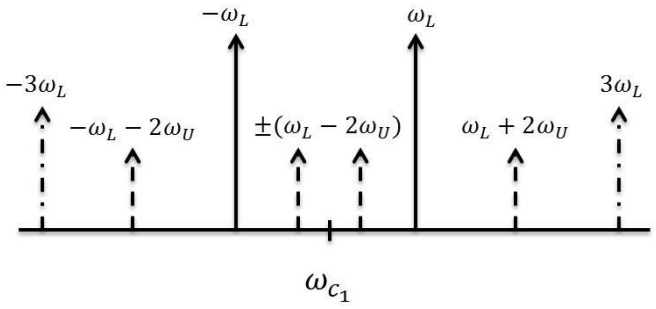

Figure 5.1: Illustration of frequency location of IM and CM products at a carrier frequency of ω_{c_1}

tone measurement was made on a concurrent dual-band RF PA, but no power and frequency sweeps were made. In this chapter, a method to analyze the IM products and cross-modulation (CM) products is introduced along with the summarization of measurement results presented in paper **C**.

5.1 Analysis of IM and CM products

To analyze the memory effects in multi-channel transmitters, an approach similar to SISO two-tone measurements can be used, i.e., each band can be excited with the two-tone signals which are symmetric around their respective carrier frequencies. Moreover, these two-tone test signals should be designed such that $\Delta\omega_L > \Delta\omega_U$ or vice versa, where $\Delta\omega_L$ and $\Delta\omega_U$ are the upper and lower angular frequencies of two-tone signals operating at lower and upper band carrier frequencies, respectively. Angular frequencies are defined as $\Delta\omega_U = 2\pi(\Delta_f)$ and $\Delta\omega_L = 2\pi(\Delta_f + \delta_f)$, with δ_f being a constant tone difference and Δ_f a varying tone difference. Figure 5.1 illustrates the frequency locations of IM and CM products.

The difference in the tone spacing of upper and lower two-tone signals is essential to differentiate between the IM and CM products, and to avoid overlapping. The method can also be used for the characterizing of memory effects in nonlinear MIMO transmitters, where the channels are operating at the same frequencies. In paper **C**, carrier frequencies for upper and lower bands were operating at 2.3 and 2 GHz, respectively and the frequency sweep was performed between 100 kHz and 10 MHz. Δ_f was varying with a step size of 0.1 MHz with δ_f fixed at 100 kHz. For amplitude sweep, the step size was 0.09 dB and the input power was swept between -16 dBm and 1 dBm. The IM and CM products were analyzed graphically using classical 2-D plots and evaluated against 3:1 amplitude slope when power sweep was performance. The 3:1 slope indicate that the amplitudes of IM and CM tones are proportional to the 3^{rd} power of the input amplitude [53]. A asymmetric 3-D

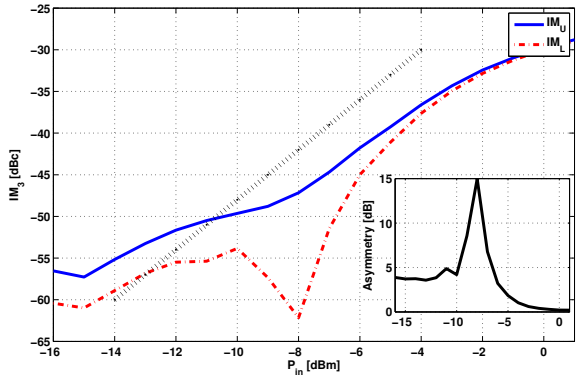

Figure 5.2: Measured amplitude of IM product relative to the carrier frequency of 2 GHz versus power sweep. A 3:1 slope is indicated by the black dotted line.

energy surfaces [52] were also used to spot region where the memory effects are more prominent.

5.2 Measurement Results

Figure 5.2 and 5.3 show the result of power sweep for IM and CM products, respectively. The dotted line indicate the 3:1 slope between -14 and -4 dBm input power. The measurement result in Figure 5.2 indicate that the amplitude of IM products is not proportional to the 3^{rd} power of input signals which indicates that the IM products are not purely due to 3^{rd} degree nonlinearities. The asymmetry between upper and lower IM products indicate memory effects. Figure 5.3 show that the lower inner and outer CM product (CM_L) approximately increases to the 3^{rd} power of input signals, where as upper inner and outer CM product (CM_U) slightly deviates from the 3:1 slope. Furthermore, Figure 5.3 indicates that both inner and outer CM products have approximately same asymmetric behavior and the asymmetry is lower compared to IM products.

The results for the frequency sweep are shown in Figure 5.4 and 5.5 for IM and CM products, respectively. Two things can clearly be observed from Figure 5.4 and 5.5, i.e., the IM products have notable memory effects than CM products as the IM products have much amplitude degradation with increase tone spacing compared to the CM products. Second, the amplitude levels of IM and CM products are different for the same input power level. In paper **C** it has been shown that the amplitude of CM products is more than the IM products by a factor of 2. Figure 5.6 shows the post processed amplitudes of IM products by taking into account the factor of 2 between the amplitudes of IM and CM products, we clearly see that the IM and CM products have approximately the same frequency dependence with

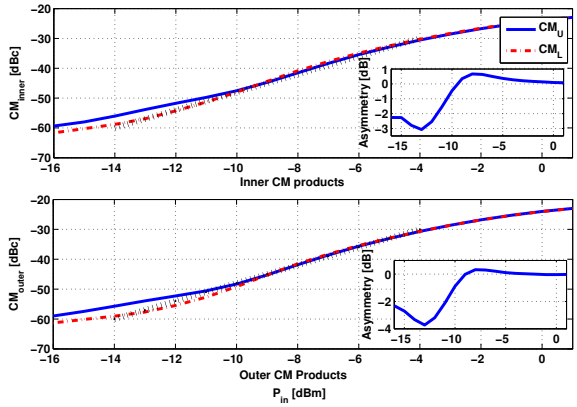

Figure 5.3: Measured amplitude of inner and outer CM products relative to the carrier frequency of 2 GHz versus power sweep. A 3:1 slope is indicated by the black dotted line.

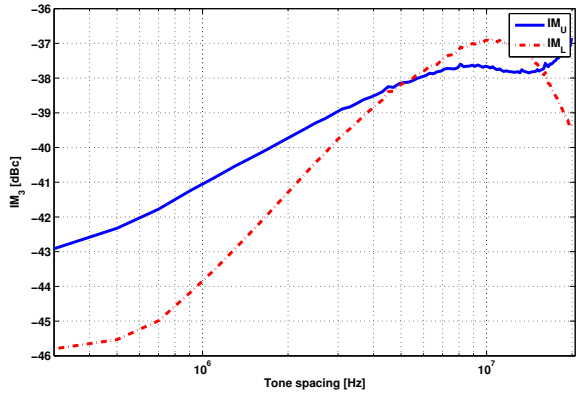

Figure 5.4: Measured amplitude of IM product as a function of frequency spacing relative to the carrier frequency of 2 GHz versus frequency sweep at $P_{in} = -6$ dBm.

increasing tone spacing compared to the results in Figure 5.4 and 5.5. Figure 5.7 show the asymmetric energy surface obtain by (3.4). Asymmetric energy surface can be utilize to highlight the frequency and power region of PAs which are sensitive to memory effects, e.g., in Figure 5.7 for a tone spacing lower than 1 MHz and for an input power less than -4 dBm, asymmetry is significant. Whereas, in some of the power and frequency region the asymmetry is zero i.e., where upper and lower

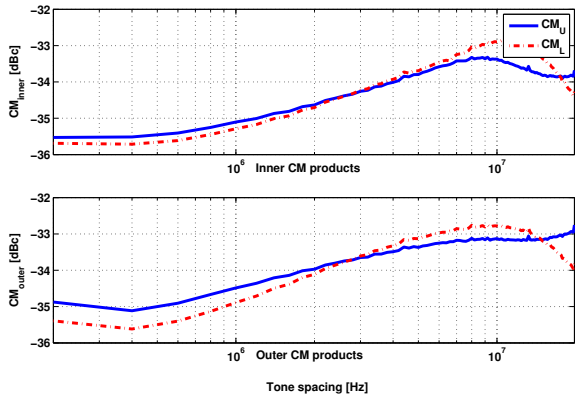

Figure 5.5: Measured amplitude of CM product as a function of frequency spacing relative to the carrier frequency of 2 GHz versus frequency sweep at $P_{in} = -6$ dBm.

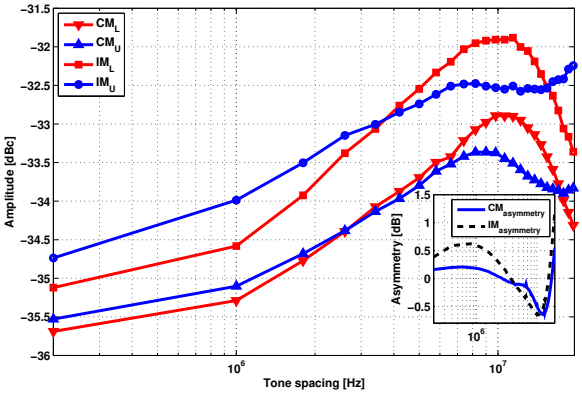

Figure 5.6: IM amplitude at -3 dBm input power level and CM amplitude at -6 dBm input power level vs tone spacing. The inset shows the amount of asymmetry between upper and lower IM and CM products.

IM products have symmetry.

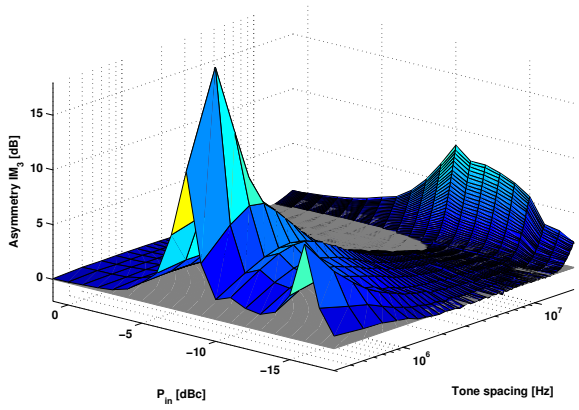

Figure 5.7: Asymmetric energy surface of IM product. Gray rectangular plan indicate symmetrical region.

Chapter 6

Conclusion

The main goal of this thesis is to develop new models for the characterization and linearization of multi-channel RF PAs. Three topics have been studied and evaluated experimentally that address some challenges faced by the multi-channel RF PAs.

The nonlinear behavior of the MIMO PAs is different compared to the SISO PAs. To model such behavior, three models proposed in paper **A** are presented and compared with the previously published 2×2 PH model for MIMO transmitters. The GMPLC model is proposed for a DUT with linear cross-talk and for behavioral modeling, the GMPLC resulted in an NMSE and ACEPR of −50.1 and −58.9-dB, respectively, and is 9 dB lower in NMSE compared to the 2×2 PH model and 2.3 dB lower in terms of ACEPR. When used as a pre-inverse model for DUT with nonlinear cross-talk, the GMPLC resulted in an ACPR of −58 dB and an NMSE of approximately −45 dB. For behavioral modeling of DUTs with nonlinear and nonlinear & linear cross-talk, the GMPNLC and EGMPNLC models are proposed. Similarly, when used as a pre-inverse model for a DUT with linear or nonlinear & linear cross-talk, both GMPNLC and EGMPNLC resulted in adequate performance compared to the 2×2 PH model. Therefore, for different cross-talk types the selection of a correct model is essential to have sufficient behavioral modeling and DPD performance. Moreover, the effect of coherent and partially non-coherent signal generation on the performance of the DPD algorithm is also highlighted, where non-coherent signal generation resulted in the degradation of DPD performance. Such effects are also present in the SISO signal generation but are more pronounced in multi-channel systems.

The behavioral models for multi-channel PAs contain a large number of model parameters compared to the SISO behavioral models. The increased number of model parameters are due to the presence of cross-terms and reduced kernel symmetry, thus, the implementation complexity increases. Therefore, the DPD of multi-channel PAs exacerbate the need for model reduction techniques. The measurement results discussed in chapter 4 show that with the implementation of sparse tech-

niques presented in paper **B**, it is possible to have a working sparse DPD model for multi-channel PAs with performance comparable to that of the corresponding dense models.

A technique for characterization of memory effects in concurrent dual-band PAs has been proposed and can easily be adapted to MIMO PAs. It is an extension of a conventional two-tone test which is extensively used in the characterization of SISO PAs. For concurrent dual-band PAs, a two-tone signal is injected into each channel and the frequency separation of one of the two-tone test signal is slightly higher in one of the channels. This frequency separation is essential to differentiate between IM and CM products. Furthermore, asymmetric energy surfaces are introduced also for CM products. These can be used to identify the power and frequency regions where the memory effects are dominant in IM and CM products. Since the method characterizes the memory effects of IM and CM products, this information can be utilized for tuning parametric DPD models in terms of memory depth and nonlinear order.

Bibliography

[1] F. C. Lanzani, G. Kardaras, and D. Boppana, "Remode radio heads and the evolution towards 4G networks," *MTI Radiocomp and Altera*, vol. 3, 2009.

[2] M. Iwamoto, A. Williams, P.-F. Chen, A. Metzger, L. Larson, and P. Asbeck, "An extended doherty amplifier with high efficiency over a wide power range," *IEEE Trans. Microw. Theory Techn.*, vol. 49, no. 12, pp. 2472–2479, Dec 2001.

[3] I. Kim, J. Moon, S. Jee, and B. Kim, "Optimized design of a highly efficient three-stage Doherty PA using gate adaptation," *IEEE Trans. Microw. Theory Techn.*, vol. 58, no. 10, pp. 2562–2574, Oct 2010.

[4] A. Grebennikov, "A high-efficiency 100-W four-stage doherty GaN HEMT power amplifier module for WCDMA systems," in *IEEE MTT-S Int. Microw. Symp.*, June 2011, pp. 1–1.

[5] Y. Li, J. Lopez, C. Schecht, R. Wu, and D. Lie, "Design of high efficiency monolithic power amplifier with envelope-tracking and transistor resizing for broadband wireless applications," *IEEE J. Solid-State Circuits*, vol. 47, no. 9, pp. 2007–2018, Sept 2012.

[6] R. Wu, Y.-T. Liu, J. Lopez, C. Schecht, Y. Li, and D. Lie, "High-efficiency silicon-based envelope-tracking power amplifier design with envelope shaping for broadband wireless applications," *IEEE J. Solid-State Circuits*, vol. 48, no. 9, pp. 2030–2040, Sept 2013.

[7] P. N. Landin, K. Barbe, W. Van Moer, M. Isaksson, and P. Handel, "Two novel memory polynomial models for modeling of RF power amplifiers," *International Journal of Microwave and Wireless Technologies*, pp. 1–11, 4 2014.

[8] P. Landin, M. Isaksson, and P. Handel, "Comparison of evaluation criteria for power amplifier behavioral modeling," in *IEEE MTT-S Int. Microw. Symp*, 2008, pp. 1441–1444.

[9] J. Pedro and S. Maas, "A comparative overview of microwave and wireless power-amplifier behavioral modeling approaches," *IEEE Trans. Microw. Theory Tech.*, vol. 53, no. 4, pp. 1150–1163, April 2005.

[10] J. Wood, *Behavioral Modeling and Linearization of RF Power Amplifiers*. Artech House, 2014.

[11] D. Schreurs, M. O'Droma, A. Goacher, and G. M., *RF Power Amplifier Behavioral Modeling*. Cambridge University Press, 2008.

[12] M. Isaksson, D. Wisell, and D. Ronnow, "A comparative analysis of behavioral models for RF power amplifiers," *IEEE Trans. Microw. Theory Techn.*, vol. 54, no. 1, pp. 348–359, 2006.

[13] M. Schetzen, "Theory of P^{th}-order inverses of nonlinear systems," *IEEE Trans Circuits Syst.*, vol. 23, no. 5, pp. 285–291, 1976.

[14] D. Mirri, G. luculano, F. Filicori, G. Pasini, G. Vannini, and G. Gabriella, "A modified Volterra series approach for nonlinear dynamic systems modeling," *IEEE Trans. Circuits Syst. I; Fundam. Theory Appl.*, vol. 49, no. 8, pp. 1118–1128, Aug 2002.

[15] A. Zhu and T. Brazil, "Behavioral modeling of RF power amplifiers based on pruned volterra series," *IEEE Microw. Compon. Lett.*, vol. 14, no. 12, pp. 563–565, Dec 2004.

[16] M. Isaksson, D. Wisell, and D. Ronnow, "Wide-band dynamic modeling of power amplifiers using radial-basis function neural networks," *IEEE Trans. Microw. Theory Techn.*, vol. 53, no. 11, pp. 3422–3428, Nov 2005.

[17] F. Mkadem, M. Ayed, S. Boumaiza, J. Wood, and P. Aaen, "Behavioral modeling and digital predistortion of power amplifiers with memory using two hidden layers artificial neural networks," in *IEEE MTT-S Int. Microw. Symp.*, May 2010, pp. 656–659.

[18] D. Morgan, Z. Ma, J. Kim, M. Zierdt, and J. Pastalan, "A Generalized Memory Polynomial model for digital predistortion of RF power amplifiers," *IEEE Trans. Signal Process.*, vol. 54, no. 10, pp. 3852–3860, Oct 2006.

[19] M. Isaksson and D. Ronnow, "A kautz-volterra behavioral model for RF power amplifiers," in *IEEE MTT-S Int. Microw. Symp.*, June 2006, pp. 485–488.

[20] J. Zhai, J. Zhou, L. Zhang, J. Zhao, and W. Hong, "Dynamic behavioral modeling of power amplifiers using ANFIS-based Hammerstein," *IEEE Microw. Compon. Lett.*, vol. 18, no. 10, pp. 704–706, Oct 2008.

[21] D. Rönnow, D. Wisell, and M. Isaksson, "Three-Tone characterization of nonlinear memory effects in Radio-Frequency power amplifiers," *IEEE Trans. Instr. and Meas.*, vol. 56, no. 6, pp. 2646–2657, Dec 2007.

[22] D. Wisell, B. Rudlund, and D. Rönnow, "Characterization of memory effects in power amplifiers using digital two-tone measurements," *IEEE Trans. Instr. and Meas.*, vol. 56, no. 6, pp. 2757–2766, Dec 2007.

[23] J. Vuolevi, T. Rahkonen, and J. Manninen, "Measurement technique for characterizing memory effects in RF power amplifiers," *IEEE Trans. Microw. Theory Techn.*, vol. 49, no. 8, pp. 1383–1389, Aug 2001.

[24] H. Ku, M. Mckinley, and J. Kenney, "Quantifying memory effects in RF power amplifiers," *IEEE Trans. Microw. Theory Techn.*, vol. 50, no. 12, pp. 2843–2849, Dec 2002.

[25] K. Remley, D. Williams, D. M. M. P. Schreurs, and J. Wood, "Simplifying and interpreting two-tone measurements," *IEEE Trans. Microw. Theory Techn.*, vol. 52, no. 11, pp. 2576–2584, Nov 2004.

[26] J. Martins, P. Cabral, N. Carvalho, and J. Pedro, "A metric for the quantification of memory effects in power amplifiers," *IEEE Trans. Microw. Theory Techn.*, vol. 54, no. 12, pp. 4432–4439, Dec 2006.

[27] D. Saffar, N. Boulejfen, F. Ghannouchi, A. Gharsallah, and M. Helaoui, "Behavioral modeling of MIMO nonlinear systems with multivariable polynomials," *IEEE Trans. Microw. Theory Techn.*, vol. 59, no. 11, pp. 2994–3003, 2011.

[28] S. Bassam, M. Helaoui, and F. Ghannouchi, "Crossover digital predistorter for the compensation of crosstalk and nonlinearity in MIMO transmitters," *IEEE Trans. Microw. Theory Techn.*, vol. 57, no. 5, pp. 1119–1128, 2009.

[29] J. Moon, P. Saad, J. Son, C. Fager, and B. Kim, "2-D enhanced Hammerstein behavior model for concurrent dual-band power amplifiers," in *42nd European Microwave Conference (EuMC)*, 2012, pp. 1249–1252.

[30] Y.-J. Liu, W. Chen, J. Zhou, B.-H. Zhou, and F. Ghannouchi, "Digital predistortion for concurrent dual-band transmitters using 2-D modified memory polynomials," *IEEE Trans. Microw. Theory Techn.*, vol. 61, no. 1, pp. 281–290, 2013.

[31] A. Swain and S. Billings, "Generalized frequency response function matrix for MIMO non-linear systems," *Int. J. Control*, pp. 829–844, 2001.

[32] C. Eun and E. Powers, "A new Volterra predistorter based on the indirect learning architecture," *IEEE Trans. Signal Process.*, vol. 45, no. 1, pp. 223–227, 1997.

[33] D. Zhou and V. E. DeBrunner, "Novel adaptive nonlinear predistorters based on the direct learning algorithm," *IEEE Trans. Signal Process.*, vol. 55, no. 1, pp. 120 –133, January 2007.

[34] A. Nasser, M. Fikri, and K. Kafrawy, "Volterra series analysis of intermodulation distortion in second-order active filters," *Circuits Systems Magazine*, vol. 5, no. 2, pp. 4–8, June 1983.

[35] H. Salgado and J. O'Reilly, "Volterra series analysis of distortion in semiconductor laser diodes," *IEE Proceedings J Optoelectronics*, vol. 138, no. 6, pp. 379–382, Dec 1991.

[36] J. Kim and K. Konstantinou, "Digital predistortion of wideband signals based on power amplifier model with memory," *Electron. Lett.*, vol. 37, no. 23, pp. 1417–1418, 2001.

[37] H. Ku and J. Kenney, "Behavioral modeling of nonlinear RF power amplifiers considering memory effects," *IEEE Trans. Microw. Theory Techn.*, vol. 51, no. 12, pp. 2495–2504, Dec 2003.

[38] T. Cunha, E. Lima, and J. Pedro, "Validation and physical interpretation of the power-amplifier polar Volterra model," *IEEE Trans. Microw. Theory Techn.*, vol. 58, no. 12, pp. 4012–4021, 2010.

[39] S. Afsardoost, T. Eriksson, and C. Fager, "Digital predistortion using a vector-switched model," *IEEE Trans. Microw. Theory Techn.*, vol. 60, no. 4, pp. 1166–1174, April 2012.

[40] M. Isaksson and D. Rönnow, "A parameter-reduced Volterra model for dynamic RF power amplifier modeling based on orthonormal basis functions," *Int. J. RF and Microw Comp Aid Eng, 17*, pp. 542–551, 2007.

[41] A. Zhu and T. Brazil, "Behavioral modeling of RF power amplifiers based on pruned Volterra series," *IEEE Microw. Wireless Compon. Lett.*, vol. 14, no. 12, pp. 563–565, 2004.

[42] F. Ghannouchi, M. Younes, and M. Rawat, "Distortion and impairments mitigation and compensation of single- and multi-band wireless transmitters," *IET Microw. Antennas Propag.*, vol. 7, no. 7, 2013.

[43] F. Dai, Y. Shi, J. Yan, and X. Hu, "MIMO RFIC Transceiver Designs for WLAN Applications," in *7th International Conference on ASIC, ASICON '07.*, Oct 2007, pp. 348–351.

[44] Y. Palaskas, A. Ravi, S. Pellerano, B. Carlton, M. Elmala, R. Bishop, G. Banerjee, R. Nicholls, S. Ling, N. Dinur, S. Taylor, and K. Soumyanath, "A 5-GHz 108-Mb/s 2x2 MIMO Transceiver RFIC With Fully Integrated 20.5-dbm P_1dB power amplifiers in 90-nm CMOS," *IEEE J. Solid-State Circuits*, vol. 41, no. 12, pp. 2746–2756, 2006.

[45] W. Chen, S. Bassam, X. Li, Y. Liu, K. Rawat, M. Helaoui, F. Ghannouchi, and Z. Feng, "Design and Linearization of Concurrent Dual-Band Doherty power amplifier with frequency-dependent power ranges," *IEEE Trans. Microw. Theory Techn.*, vol. 59, no. 10, pp. 2537–2546, Oct 2011.

[46] P. Saad, P. Colantonio, L. Piazzon, F. Giannini, K. Andersson, and C. Fager, "Design of a concurrent dual-band 1.8 and 2.4-GHz GaN-HEMT Doherty power amplifier," *IEEE Trans. Microw. Theory Techn.*, vol. 60, no. 6, pp. 1840–1849, June 2012.

[47] T. Öberg, *Modulation Detection and Coding.* West Sussex, England: John Wiley & Sons, 2001.

[48] S. Kay, *Fundamentals of Statistical Signal Processing: Estimation Theory.* Upper Saddle River, New Jersey, USA: Prentice-Hall PTR, 1998.

[49] S. Amin, E. Zenteno, P. Landin, D. Ronnow, M. Isaksson, and P. Handel, "Noise impact on the identification of digital predistorter parameters in the indirect learning architecture," in *Swedish Communication Technologies Workshop (Swe-CTW)*, 2012, pp. 36–39.

[50] P. Landin, A. Mayer, and T. Eriksson, "MILA - A noise mitigation technique for RF power amplifier linearization," in *IEEE International Multi-Conference on Systems, Signals Devices (SSD)*, Feb 2014, pp. 1–4.

[51] "IEEE standard for terminology and test methods for analog-to-digital converters," *IEEE Std 1241-2010 (Revision of IEEE Std 1241-2000)*, pp. 1–139, January 2011.

[52] W. Van Moer and Y. Rolain, "A large-signal network analyzer: Why is it needed?" *IEEE Microw. Mag.*, vol. 7, no. 6, pp. 46–62, 2006.

[53] V. Joel and R. Timo, *Distortion in RF Power Amplifiers.* Boston London: Artech Hourse, 2003.

[54] M. Herman, B. Miller, and J. Goodman, "The cube coefficient subspace architecture for nonlinear digital predistortion," in *42nd Asilomar Conference on Signals, Systems and Computers, 2008*, 2008, pp. 1857–1861.

[55] J. Reina-Tosina, M. Allegue-Martinez, M. Madero-Ayora, C. Crespo-Cadenas, and S. Cruces, "Digital predistortion based on a compressed-sensing approach," in *European Microwave Conference*, Oct. 2013, pp. 408–411.

[56] A. Abdelhafiz, A. Kwan, O. Hammi, and F. Ghannouchi, "Digital predistortion of LTE-A power amplifiers using Compressed-Sampling-Based unstructured pruning of Volterra series," *IEEE Trans. Microw. Theory Techn.*, vol. PP, no. 99, pp. 1–11, 2014.

[57] J. Li, K. Das, G. Fu, R. Li, and R. Wu, "The bayesian LASSO for genome-wide association studies," *Bioinformatics*, vol. 27, no. 4, pp. 516–523, 2011. [Online]. Available: http://bioinformatics.oxfordjournals.org/content/27/4/516.abstract

[58] A. Motyer, C. McKendry, S. Galbraith, and S. Wilson, "LASSO model selection with post-processing for a genome-wide association study data set," *BMC Proceedings*, vol. 5, no. Suppl 9, p. S24, 2011. [Online]. Available: http://www.biomedcentral.com/1753-6561/5/S9/S24

[59] V. Kekatos and G. Giannakis, "Sparse Volterra and Polynomial Regression Models: Recoverability and Estimation," *IEEE Trans. Signal Process.*, vol. 59, no. 12, pp. 5907–5920, Dec 2011.

[60] D. Wisell, J. Jalden, and P. Handel, "Behavioral power amplifier modeling using the LASSO," in *IEEE IMTC 2008*, May 2008, pp. 1864–1867.

[61] M. Grant and S. Boyd, "Graph implementations for nonsmooth convex programs," in *Recent Advances in Learning and Control*, ser. Lecture Notes in Control and Information Sciences, V. Blondel, S. Boyd, and H. Kimura, Eds. Springer-Verlag Limited, 2008, pp. 95–110.

[62] D. M. Pozar, *Microwave Engineering, 4th ed.* Hoboken, NJ, USA: John Wiley, 2011.

[63] J. Pedro and J. Martins, "Amplitude and phase characterization of nonlinear mixing products," *IEEE Trans. Microw. Theory Techn.*, vol. 54, no. 8, pp. 3237–3245, Aug 2006.

[64] W. Chen, S. Bassam, X. Li, Y. Liu, K. Rawat, M. Helaoui, F. Ghannouchi, and Z. Feng, "Design and linearization of concurrent dual-band Doherty power amplifier with frequency-dependent power ranges," *IEEE Trans. Microw. Theory Techn.*, vol. 59, no. 10, pp. 2537–2546, Oct 2011.

Part II

Included papers